COBRA: COllaborative Bot with multi-Rotor Actuation

Camilo Ordonez[1], Oscar Chuy[2] and Tomas Fajardo[1]

***Abstract*— Wheeled robots operating in the field are faced with mobility challenges such as drop-offs, slippery slopes, and cluttered environments. In these situations, it is desirable to have agile and highly mobile platforms. This paper explores the utilization of multiple rotors to enhance the mobility of ground vehicles. A strategy based on downward thrust generation is developed to increase traction and surmount otherwise non-traversable slippery inclines. Both simulation and experimental results are presented to show the efficacy of the proposed solution.**

I. INTRODUCTION

Off-road wheeled vehicles are the platforms of choice in many applications because they can navigate difficult terrains while carrying sufficient payload. When navigating outdoor scenarios, robots are regularly faced with difficult mobility challenges such as drop-offs, steep hills, patches of ice, snow, and mud. One approach to navigate difficult terrains consists of the development of hybrid platforms that can fly and roll [1], [2], [3]. These systems fly as conventional quadrotors and roll employing a tilt mechanism and passive wheels. However, in order to achieve aerial and terrestrial locomotion, they are constrained to small payloads. In addition, due to the passive wheels, they suffer from limited maneuverability on the ground, which makes it difficult to follow prescribed vehicle trajectories.

From the mobility challenges listed above, slippery surfaces and hills are one of the most pervasive and therefore researchers have developed traction control approaches. Most solutions detect the onset of slippage and regulate the torque being applied to the wheels to reduce the vehicle acceleration and reduce slippage [4], [5], [6], [7].

Model Following Control (MFC) [8], MFC's variant [9] and Maximum Transferable Torque Estimate (MTTE) [10], [11], [12] have been implemented to mitigate slip on electric vehicles. These approaches do not depend on vehicle chassis velocity but do employ vehicle model and input torque to the wheel to detect slip. MFC and MTTE are advanced control approaches in slip mitigation. They require complex setups where input torque is available. In addition, they heavily rely on the vehicle's dynamic model.

The above approaches are limited to work in situations where there is enough normal force to generate tractive force. In this work, a different approach is taken. The proposed solution relies on the cooperation of an air vehicle with a wheeled platform to regulate the normal forces acting on each of the wheels. It is important to emphasize that the intention here is to use the air/ground cooperation to overcome difficult maneuvers that the wheeled robot can not overcome on its own. The idea is not to have a combined flying/rolling system. As depicted in Fig. 1, we envision that in a fielded system the cooperation between the robots would take place only at critical points of the robotic mission.

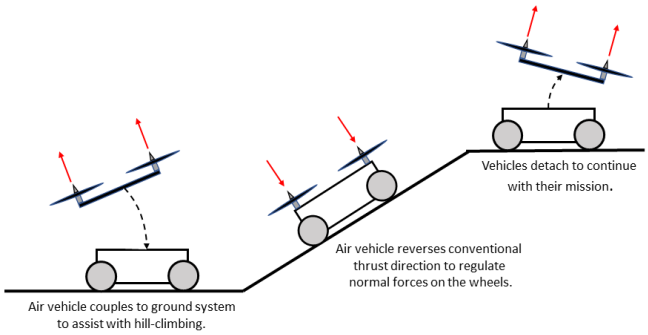

Fig. 1. Air/ground robot cooperation to overcome a steep slippery incline.

By controlling the normal forces, the ground vehicle is capable to traverse otherwise non-traversable, steep and slippery hills. The developed platform shown in Fig. 2 is called COBRA (COllaborative Bot with multi-Rotor Actuation). This paper focuses on traction control. However, as illustrated in Fig. 3, the proposed rotor/wheel cooperation scheme is expected to add agility and aid in diverse maneuvers such as 3-dimensional mid-air self-righting (see video for preliminary results), reducing the vehicle minimum turn radius, and minimizing rollover risk during high speed

Fig. 2. The COBRA platform.

*This work was not supported by any organization

[1]Camilo Ordonez and Tomas Fajardo are with the Department of Mechanical Engineering at the FAMU-FSU College of Engineering, Tallahassee FL 32310, USA cordonez@fsu.edu

[2]Oscar Chuy is with the Department of Electrical Engineering at the FAMU-FSU College of Engineering, Tallahassee, FL 32310, USA chuy@eng.famu.fsu.edu

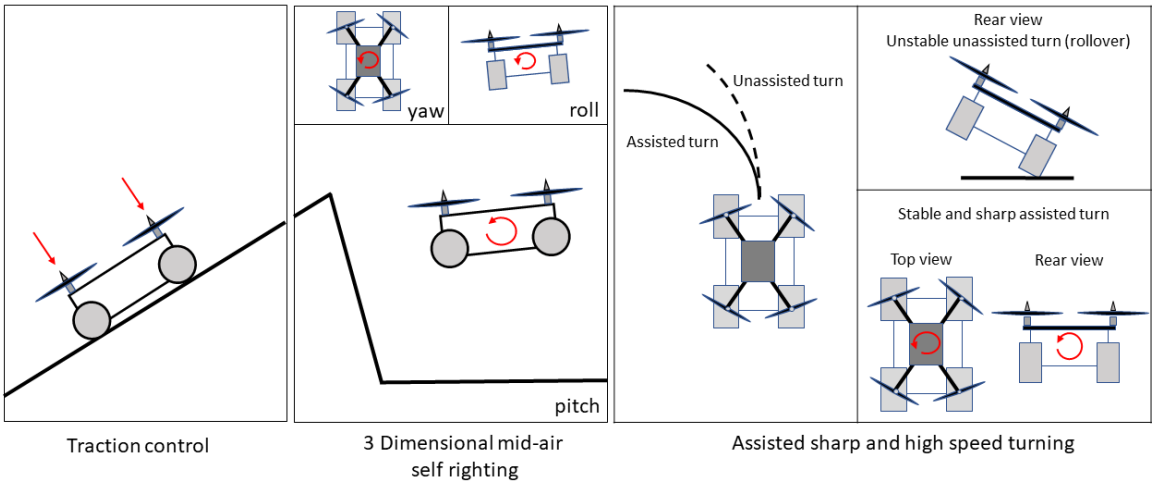

Fig. 3. Increased agility and mobility due to cooperative actuation of rotors and wheels.

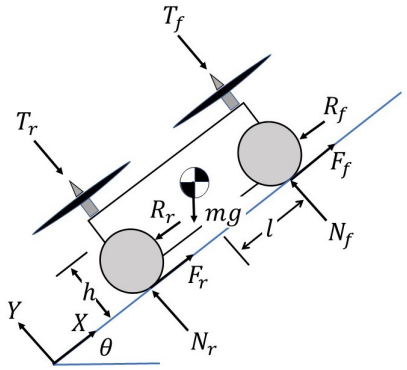

Fig. 4. Free-body diagram of the system climbing a hill.

turning. Note that it has been shown in [13], [14], [15] that manipulation of downward force greatly affects and aids vehicle handling, stability and safety. However, the approaches in [13], [14], [15] are only applicable at high speeds. Related work to climbing of vertical surfaces is included in [16]. This platform was designed to inspect petrochemical vessels. To generate attachment to the walls, the robot employs two coaxial upturned propellers (right and left handed). However, that work relies on an open loop strategy to maintain adhesion, which can be energy inefficient. Furthermore, the robot configuration is limited to climbing scenarios. An additional robot capable of driving and flying is developed in [17]. However, that work was not concerned with climbing.

The remainder of the paper is structured as follows: Section II details the experimental platform. Section III develops the dynamic model of the system. Section IV presents simulation findings. Section V includes experimental results. Finally, Section VI provides conclusions and avenues for future work.

TABLE I

NOMENCLATURE

Parameter	Symbol	Value	Units
System mass	m	6.71	kg
Wheel radius	r_w	0.073	m
Vehicle half length	l	0.26	m
Height of center of gravity	h	0.10	m
Front propeller thrust force	T_f	30 Max	N
Rear propeller thrust force	T_r	30 Max	N
Propeller radius	r_p	6	$inch$
Propeller pitch	p	4.5	$inch$
Front tractive force	F_f	variable	N
Rear tractive force	F_r	variable	N
Front normal force	N_f	variable	N
Rear normal force	N_r	variable	N
Vehicle velocity	$\dot{x}$	variable	$\frac{m}{s}$
Vehicle acceleration	$\ddot{x}$	variable	$\frac{m}{s^2}$
Desired Vehicle velocity	$\dot{x}_d$	variable	$\frac{m}{s}$
Coefficient of rolling resistance	μ_{rr}	variable	-
Front rolling resistance	R_f	variable	N
Rear rolling resistance	R_r	variable	N
Front wheel torque	τ_f	variable	Nm
Rear wheel torque	τ_r	variable	Nm
Hill grade	θ	variable	rad
Wheel velocity	ω	variable	$\frac{rad}{sec}$
Desired Wheel velocity	ω_d	variable	$\frac{rad}{sec}$
Slip ratio	k	variable	%
Pacejka model coefficients	B, C, D, E	variable	-

TABLE II

PACEJKA MODEL COEFFICIENTS

Surface	B	C	D	E
Dry Tarmac	10.0	1.9	1.0	0.97
Wet Tarmac	12.0	2.3	0.82	1.0
Ice	4.0	2.0	0.1	1.0
Soapy Aluminum	4.0	2.0	0.29	1.0

II. EXPERIMENTAL PLATFORM

The experimental platform consists of an off the shelf RC(radio controlled) vehicle. The axles of the vehicle were extended to add wheel encoders on each of the wheels. These encoders are used to calculate the wheel velocities. In addition, a carbon fiber body on top of the vehicle was designed to hold the arms of the multirotor system. Each

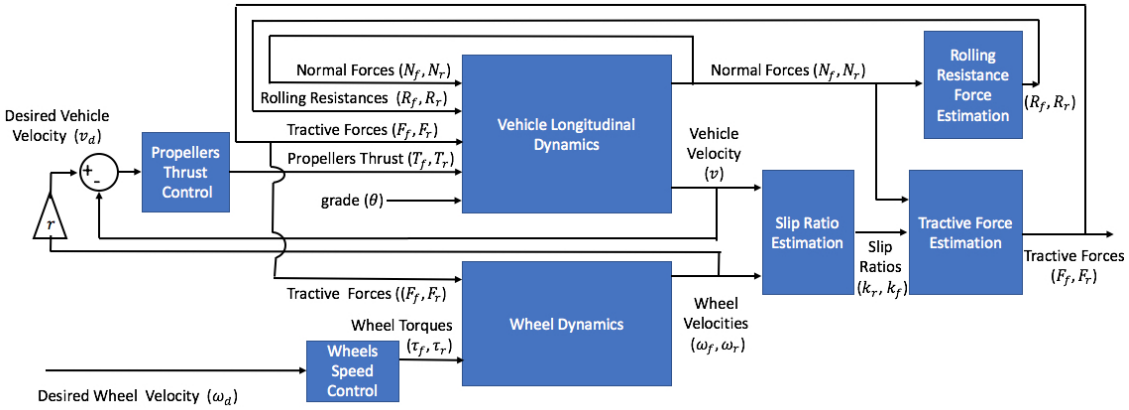

Fig. 5. Block diagram of the dynamic model and its control.

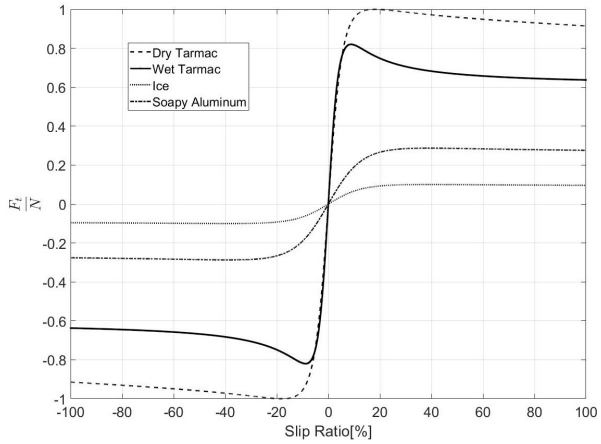

Fig. 6. Tractive force for different surfaces.

rotor is driven by a COBRA CM3515 brushless motor with a 12x4.5 propeller.

The vehicle is controlled in real-time with an ATMEL Mega 2560 microcontroller at a rate of 100Hz. The real-time implementation is based on a timer that executes an interrupt service routine every 10 ms. The encoders signals are decoded through software with the use of external interrupts. The vehicle accelerations are read using a BNO055 6DOF IMU (Inertial Measurement Unit) [18]. Using numerical integration, the velocity of the vehicle is obtained. In addition, an SD card is employed to store experimental data. The main platform characteristics and nomenclature used throughout the paper are summarized in Table I.

III. DYNAMIC MODELING

A free-body diagram of the robot climbing a hill is presented in Fig. 4. The main forces acting on the vehicle are the weight mg, the rear and front normal forces N_r and N_f, the tractive forces F_r and F_f, the rolling resistances R_r and R_f, and the thrust forces generated by the propellers T_r and T_f. The longitudinal dynamics of the vehicle are given by

$$F_r + F_f - R_r - R_f - mg\sin\theta = m\ddot{x}, \tag{1}$$

where the rolling resistances are estimated as:

$$R_r + R_f = \mu_{rr}(N_r + N_f), \tag{2}$$

with μ_{rr} being the coefficient of rolling resistance. The normal forces can be computed by performing moment balances about the rear and front wheels and are given by

$$N_f = \frac{-mh\ddot{x} + mgl\cos\theta - mgh\sin\theta + 2lT_f}{2l}, \tag{3}$$

$$N_r = \frac{mh\ddot{x} + mgl\cos\theta + mgh\sin\theta + 2lT_r}{2l}. \tag{4}$$

Notice that as shown in (3) and (4), the normal forces can be regulated by commanding downward thrusts to the propellers.

As described in [19], [20], [21], the tractive forces can be estimated as a function of the vehicle slip ratio using the Pacejka model [22], which estimates the tractive force F_t as a function of the vehicle slip ratio k and the normal force on the tire N

$$F_t = ND\sin(C\tan^{-1}(Bk - E(Bk - \tan^{-1}(Bk)))), \tag{5}$$

where B,C,D, and E are coefficients determined empirically for different surfaces and are summarized in Table II.

The subindex $_t$ in (5) refers to either the front $_f$ or rear $_r$ wheels. The slip ratio is computed during acceleration as $k = \frac{r_w\omega - \dot{x}}{\dot{x}}$, where r_w is the wheel radius, ω the wheel angular velocity, and $\dot{x}$ the vehicle forward velocity. Figure 6 illustrates tractive forces as a function of slip ratio for different surfaces.

The wheel rotational dynamics are governed by

$$\tau_i - F_i r_w = J\dot{w}_i, \tag{6}$$

where subindex i represents either the front or rear wheels, τ_i is the applied wheel torque, F_i is the tractive force, r_w the wheel radius, J the wheel inertia, and $\dot{\omega}_i$ the wheel angular acceleration.

IV. SIMULATION RESULTS

To simulate a typical hill-climbing maneuver, equations 1-6 were simulated in Matlab's Simulink environment. A block diagram of the complete system is shown in Fig. 5. A PD wheel speed controller was implemented to regulate the vehicle wheel speed. In addition, a PI control law was included to regulate the downward thrust from the rotors and

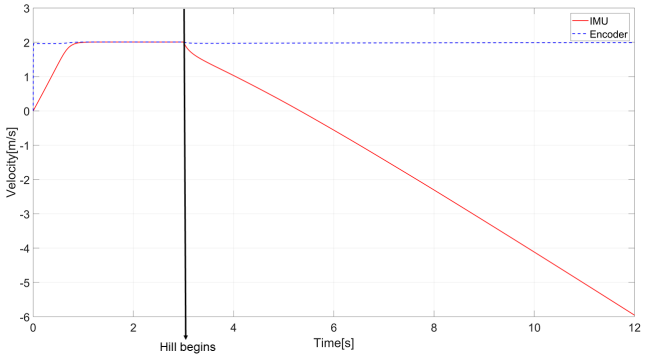

Fig. 7. Simulation results comparing encoder and IMU-based velocities of the vehicle. This simulation does not employ the thrust control, which resulted in the vehicle sliding down the hill. Hill begins is the moment when the front wheels of the vehicle are on the ramp.

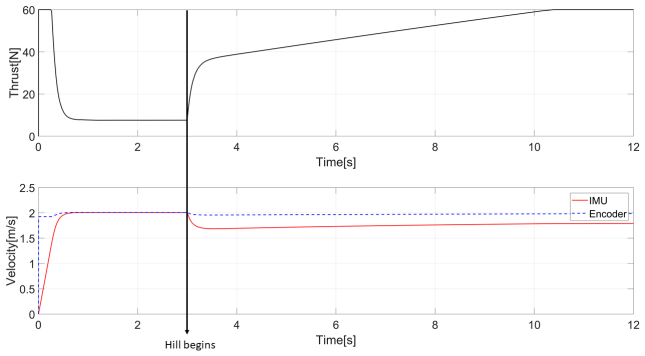

Fig. 8. Top: control effort signal of the thrust controller. Bottom: comparison of encoder and IMU-based velocities of the vehicle. This experiment employs the thrust control and the robot was able to climb the hill.

minimize slippage of the vehicle. The front T_f and rear T_r thrusts are computed using

$$T(t) = k_p e(t) + k_i \int_0^t e(\tau) d\tau, \tag{7}$$

where $e = \dot{x}_d - \dot{x}$, $\dot{x}_d$ is the desired vehicle velocity obtained from wheel encoders (i.e., assuming rolling conditions) and $\dot{x}$ is the actual vehicle velocity estimated with the IMU.

Experimentally, it was found that the maximum downward force generated by the propellers is $60N$.

A 20° slippery slope with the properties of the soapy aluminum of Fig. 6 was simulated. The robot starts moving on flat ground with a desired speed of $2m/s$ and then transitions to the slippery hill. In the first scenario the control law (7) was turned off, which, as shown in Fig. 7, resulted in excessive slip and the vehicle was not able to climb the hill. In the second simulation shown in Fig. 8, the thrust control law was engaged and the vehicle was able to climb the hill by regulating the normal forces on the wheels. Notice that the downward thrust takes on a small value during the flat portion of the experiment. This is an important feature as it reduces rolling resistance and minimizes energy consumption. As expected, there is a difference between the encoder-based and the IMU-based velocities because as predicted by (5), the tractive force is a function of slip.

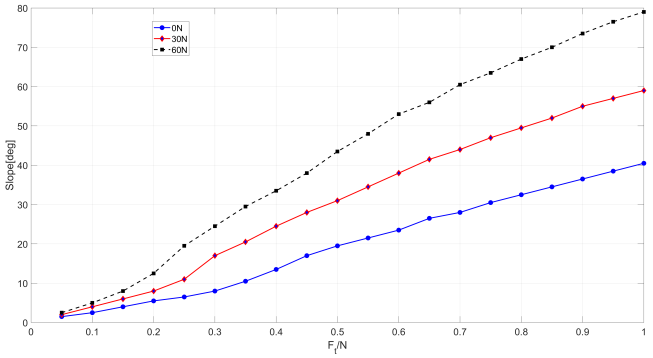

Fig. 9. Maximum climbable slope for different surfaces and levels of downward thrust.

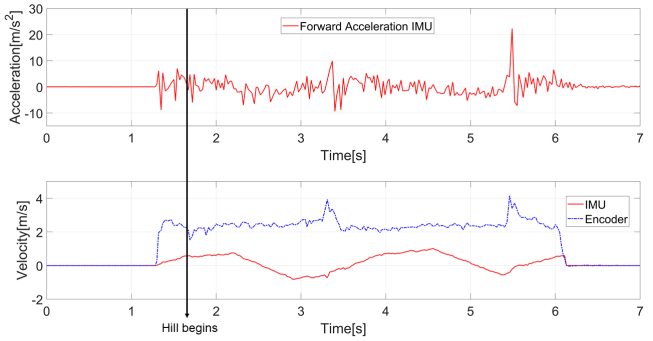

Fig. 10. Experimental result without thrust control. Top: measured acceleration from the IMU. Bottom: encoder and IMU-based velocities. Notice that the IMU velocity oscillates as the vehicle slides down the hill and attempts to climb multiple times without success.

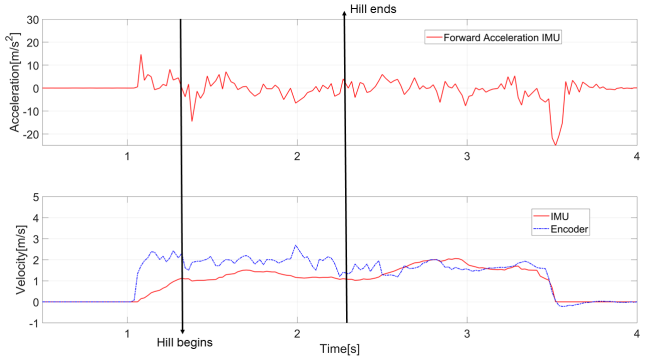

Fig. 11. Experimental result with thrust control. Top: measured acceleration from the IMU. Bottom: encoder and IMU-based velocities. Notice that the IMU velocity remains positive and the robot was able to climb the hill. Hill ends is the moment when the front wheels of the vehicle are off the ramp.

To evaluate the performance limits of the platform, Fig. 9 shows simulation results of the robot climbing slopes of different friction characteristics. This figure shows the maximum climbable slope for different levels of downward thrust.

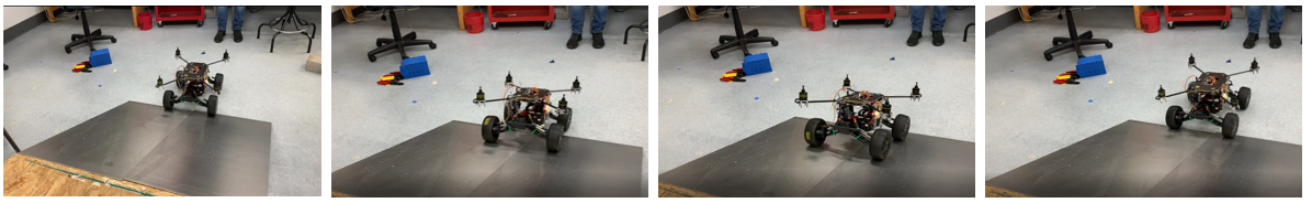

Fig. 12. Robot unsuccessfully attempting to climb a slippery 20° slope (aluminum with soap) without employing downward thrust from the propellers. The robot goes up about one body length thanks to its momentum but then it slides down the hill. The time stamps are correlated to Fig. 10.

Fig. 13. Robot successfully climbing a slippery 20° slope (aluminum with soap) by employing downward thrust from the propellers. The time stamps are correlated to Fig. 11.

Fig. 14. Experiment on a level, high-friction surface.

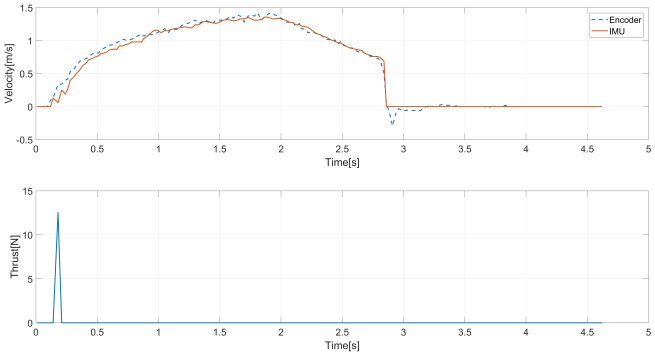

Fig. 15. Experiment on a level, high-friction surface. The downward thrust only activates during the acceleration of the vehicle at the beginning of the experiment. The propellers deactivate once the slippage becomes negligible.

V. EXPERIMENTAL RESULTS

To validate the approach experimentally, a 20° wooden ramp was constructed and two aluminum plates were placed on the rise of the ramp. The surface was made slippery by applying a solution of soapy water on top of the aluminum. This type of surface allows for controlled experimentation and is expected to behave similar to real-world surfaces such as icy surfaces or other slippery terrains. In the first experiment, the multi-rotors were not employed. As observed in Figs. 10 and 12 the robot climbed only a small portion of the hill and slid down due to excessive slippage (view video for further details). In the second experiment summarized in Figs. 11 and 13, the thrust control law was engaged and the robot was able to climb the hill. Figure 11 shows the acceleration measurements and a comparison of the encoder-based and the IMU-based velocities.

In the third experiment, as shown in Fig. 14, the robot was commanded to traverse a flat, high-friction, wooden surface at constant speed. Figure 15 demonstrates that the propellers' thrust-control activates when the robot starts moving but shuts off rapidly after because there is not enough slippage.

VI. CONCLUSIONS AND FUTURE WORK

This paper developed a new methodology to traverse slippery surfaces through air/ground vehicle cooperation. The normal forces on the wheels of the ground vehicle are controlled through multi-rotor actuation. The proposed approach was validated in simulation and experimentally in the developed COBRA platform.

While this paper focused on steep hills, the multi-rotor approach opens multiple possibilities to increase maneuverability of ground vehicles. For example, by reversing the thrust vectors, it is possible to perform self-righting maneuvers in preparation for landing after a jump (see video for preliminary results). Future work will involve a study of rapid turning maneuvers and minimization of rollover through thrust actuation. Finally, we seek to study integration of wheel-based traction control approaches with the one here proposed.

ACKNOWLEDGMENT

Special thanks to Benjamin Bazyler for the fabrication and first iteration of the platform, Diego Gonzalez for his contributions with preliminary experiments and Ryan Alicea for his help with CAD drawings and initial designs.

REFERENCES

[1] S. Jeong and S. Jung, A quad-rotor system for driving and flying missions by tilting mechanism of rotors: From design to control, Mechatronics, 24(8), pp.1178-1188, 2014.

[2] J. Page and P. Pounds. The Quadroller: Modeling of a UAV/UGV Hybrid Quadrotor. IEEE/RSJ International Conference on Intelligent Robots and Systems, pp.4834-4841, 2014.

[3] A. Kalantari and M. Spenko, Modeling and Performance Assessment of the HyTAQ, a Hybrid Terrestrial/Aerial Quadrotor, IEEE Transactions on Robotics, 30(5), pp.1278-1285, 2014.

[4] K. Fujii and H. Fujimoto. Traction control based on slip ratio estimation without detecting vehicle speed for electric vehicle. In Power Conversion Conference, pp.688-693, 2007.

[5] F. Gustafsson. Slip-based tire-road friction estimation. Automatica, 33(6):1087-1099, 1997.

[6] H. Kataoka, H. Sado, I. Sakai, and Y. Hori. Optimal slip ratio estimator for traction control system of electric vehicle based on fuzzy inference. Elect. Eng. Jpn., 135:5663, 2001.

[7] B. Subudhi and S. Ge. Sliding-mode-observer-based adaptive slip ratio control for electric and hybrid vehicles. IEEE Transactions on Intelligent Transportation Systems, 13(4):1617-1626, 2012.

[8] Y. Hori, Y. Toyoda, and Y. Tsuruoka. Future vehicle driven by electricity and control research on four-wheel-motored UOT Electric March II. IEEE Transactions on Industrial Electronics, 51(5):954-962, 2004.

[9] K. Nam, Y. Hori and C. Lee, Wheel Slip Control for Improving Traction-Ability and Energy Efficiency of a Personal Electric Vehicle, Journal of Energies, pp. 6820-6840, 2015.

[10] D. Yin, S. Oh, Y. Hori, A novel traction control for ev based on maximum transmissible torque estimation, IEEE Transactions on Industrial Electronics, vol. 56, no. 6, pp. 2086-2094, 2009.

[11] D. Yin, Y. Hori, A novel traction control for electric vehicle without chassis velocity, INTECH, pp. 121-140, 2010, ISBN 978-953-7619-55-8.

[12] O. Chuy, E. Collins. C Ordonez, J. Candiotti, H. Wang and R. Cooper, Slip mitigation control for an electric powered wheelchair, IEEE International Conference on Robotics and Automation (ICRA), pp.333-338, 2014.

[13] A. Ahangarnejad and S. Melzi, Numerical analysis of the influence of an actively controlled spoiler on the handling of a sports car, Journal of Vibration and Control, 24(22), pp.5437-5448, 2018. https://doi.org/10.1177/1077546318754683

[14] A. Savkoor and H. Happel, Aerodynamic vehicle ride control with active spoilers, In: 3rd proceedings of international symposium on advanced vehicle control pp.647-682, 1996.

[15] A. Savkoor and C. Chou, Application of aerodynamic actuators to improve vehicle handling, Vehicle System Dynamics, 32(4-5), pp. 345-374, 1999.

[16] M. Alkalla, M. Fanni, A. Mohamed, S. Hashimoto, Tele-operated propeller-type climbing robot for inspection of petrochemical vessels, Industrial Robot, 44(2), pp. 166-177, 2016.

[17] B. Araki, J. Strang, S. Pohorecky, C. Qiu, T. Naegeli and D. Rus, Multi-robot Path Planning for a Swarm of Robots that Can Both Fly and Drive, IEEE International Conference on Robotics and Automation (ICRA), pp.5575-5582, 2017.

[18] https://learn.adafruit.com/adafruit-bno055-absolute-orientation-sensor/overview

[19] P. Shakouri, A. Ordys, M. Askari and D. Laila, Longitudinal vehicle dynamics using Simulink/Matlab, UKACC International Conference on Control, pp.1-6,2010.

[20] J. Y. Wong, Theory of Ground Vehicle, 3rd edition, John Wiley and Sons, Inc

[21] J. Y. Wong and C.F. Chiang, A general theory for skid steering of tracked vehicles on firm ground, Proceedings of the Institution of Mechanical Engineers, Part D, Journal of Automotive Engineering pp.343-355, 2001.

[22] H. B. Pacejka and E. Bakker, The magic formula tyre model, Vehicle System Dynamics, 21:sup001, 1-18, DOI: 10.1080/00423119208969994